Hindawi
Journal of Chemistry
Volume 2023, Article ID 2151669, 10 pages
https://doi.org/10.1155/2023/2151669

Research Article

3-(5-Hydroxyphenyl)-5-Phenyl-2-Pyrazolines as Toll-Like Receptor 7 Agonists

Ji Hwan Kim,[1] **Seunghyun Ahn**,[2] **Dongsoo Koh**,[2] **Young Han Lee**,[3,4] **Yoongho Lim**,[1] **and Soon Young Shin**[3,4]

[1]*Division of Bioscience and Biotechnology, Konkuk University, Seoul 5029, Republic of Korea*
[2]*Department of Applied Chemistry, Dongduk Women's University, Seoul 2748, Republic of Korea*
[3]*Department of Biological Sciences, Konkuk University, Seoul 5029, Republic of Korea*
[4]*Cancer and Metabolism Institute, Konkuk University, Seoul 5029, Republic of Korea*

Correspondence should be addressed to Soon Young Shin; shinsy@konkuk.ac.kr

Received 14 September 2022; Revised 31 January 2023; Accepted 18 February 2023; Published 8 March 2023

Academic Editor: Michele Benedetti

Toll-like receptor 7 (TLR7) is an attractive target for developing immune modulators to enhance innate immunity against ssRNA virus infections, including hepatitis C and COVID-19. Ten 3-(5-hydroxyphenyl)-5-phenyl-2-pyrazolines were tested using TLR7 reporter cells, overexpressing TLR7 and the NF-κB-inducible SEAP reporter gene to discover a novel TLR7 agonist enhancing innate immunity. Of these, 2-(3-(2-hydroxynaphthalen-1-yl)-5-(4-methoxyphenyl)-4,5-dihydro-1*H*-pyrazol-1-yl)thiazol-4(5H)-one (compound **6**) showed the best TLR7 agonistic activity, and further experiments were carried out to study the immune-modulatory capability of compound **6**. Treatment with compound **6** rapidly induced phosphorylation of IRAK4, IKKα/β, IκBα, and p65/RelA in THP1 monocytic cells. In addition, it increased the expression of NF-κB-regulated innate cytokines, such as TNFα and IL1β, in THP1 monocytic cells. These data suggest that compound **6** induces an innate immune response by agonizing TLR7 activity in THP1 human monocytic cells. Therefore, compound **6** can be used as an innate immune modulator to develop antiviral agents and vaccine adjuvants.

1. Introduction

The innate immune system is an immediate nonspecific immune response providing the first line of defense against invading pathogens. Toll-like receptors (TLRs) are pattern recognition receptors that sense the presence of pathogen-associated molecular patterns (PAMPs) on invading pathogens [1]. TLRs activate intracellular signaling pathways, triggering innate immunity [2, 3] and adaptive immune responses [4, 5].

Ten TLR subtypes (TLR1-10) have been identified in humans. Among them, TLR7 is an endosomal receptor that senses single-stranded (ss) RNA [6], implicating TLR7 in innate antiviral immunity. Additionally, studies using TLR7-deficient mice have demonstrated that TLR7 recognizes ssRNA viruses, including vesicular stomatitis and influenza [6]. Indeed, TLR7 agonists exert a potent immunostimulatory effect against hepatitis C virus infection [7] and help treat ssRNA virus infection [8–10]. Furthermore, the low sensitivity of the TLR7 signaling pathway has been proposed as a common denominator for vulnerable patient groups during SARS-CoV-2 infection [11]. Loss-of-function variants of the X-chromosome TLR7 caused several young patients (age < 35 years) to become seriously ill after SARS-CoV-2-infected coronavirus disease 2019 (COVID-19) [12]. In addition, the immunostimulatory ability of TLR7 agonists has been investigated as a potential vaccine adjuvant [13, 14]. These findings suggest that TLR7 is an attractive target for developing immune modulators to enhance innate immunity against ssRNA viral infections, including hepatitis C and COVID-19. Therefore, in this study, we aimed to identify a novel TLR7 agonist that enhances innate immunity to develop an antiviral agent or vaccine adjuvant.

TLR7-mediated innate immune responses are facilitated by nuclear factor kappa B (NF-κB) activation [15]. Upon ligand binding, TLR7 recruits the adaptor protein myeloid differentiation primary response 88 (MyD88), which interacts with IL-1receptor-associated kinase 4 (IRAK4) and IRAK1 [16]. The MyD88/IRAK4/IRAK1 complex associates with ubiquitin E3 ligase tumor necrosis factor receptor-associated factor 6 (TRAF6), activating the inhibitor of κB (IκB) kinase (IKK) complex, which consists of two kinases (IKKα and IKKβ) and a regulatory subunit (NF-κB essential modulator; NEMO) [17]. The activated IKK complex induces IκB degradation in the cytoplasm, leading to the translocation of NF-κB to the nucleus. Consequently, nuclear NF-κB promotes the expression of several proinflammatory cytokines, such as IL-1β and TNFα, involved in the innate immune response [18].

TLR7 ligands can be classified as natural and synthetic. Natural ligands include guanosine, uridine-rich ssRNA, and ssRNA viruses. Nucleoside analogs, such as imiquimod (R-837), resiquimod (R-848), and PF-4878691, are synthetic ligands (Supplementary Figure 1) [10, 19]. They have common features such as the presence of 2-imidazoline (Supplementary Figure 2(a)). Unlike 2-imidazoline, in which two nitrogen atoms are separated by carbon, 2-pyrazoline (Supplementary Figure 2(b)) contains two neighboring nitrogen atoms. In resiquimod, oxygen is located at a distance of 2.8 Å and 3.5 Å from nitrogen (Supplementary Figure 3(a)); for 3-(5-hydroxyphenyl)-5-phenyl-2-pyrazoline, oxygen occurs at a distance of 2.6 Å and 3.8 Å from nitrogen (Supplementary Figure 3(b)). Structure-activity relationships of TLR7 agonists reveal that pharmacophores, including hydrogen bonding, stacking interactions, hydrophobic, and van der Waals interactions, are required for good agonism [20]. As shown in Figure 1, 3-(5-hydroxyphenyl)-5-phenyl-2-pyrazolines demonstrated hydrogen bonding, stacking, and hydrophobic interaction groups. They have 2-pyrazoline moiety instead of 2-imidazoline included in imiquimod and resiquimod, but the distance between oxygen and nitrogen is similar to that of 2-imidazoline. Therefore, they were expected to exhibit TLR7 agonism.

In this study, we evaluated whether ten 3-(5-hydroxyphenyl)-5-phenyl-2-pyrazolines exert TLR7 agonistic activity in THP1 monocytic cells, which are used extensively to study innate immunity [21].

2. Materials and Methods

2.1. Preparation of 3-(5-Hydroxyphenyl)-5-phenyl-2-pyrazolines. The structures of 3-(5-hydroxyphenyl)-5-phenyl-2-pyrazolines are shown in Figure 2.

The synthetic scheme for compounds **1**, **2**, **3**, and **10** is shown in Supplementary Figure 4 and their spectroscopic data are described as follows:

$$5-(\text{naphthalene}-1-yl)-3-(2-\text{hydroxyphenyl})\text{pyrazoline}. \quad (1)$$

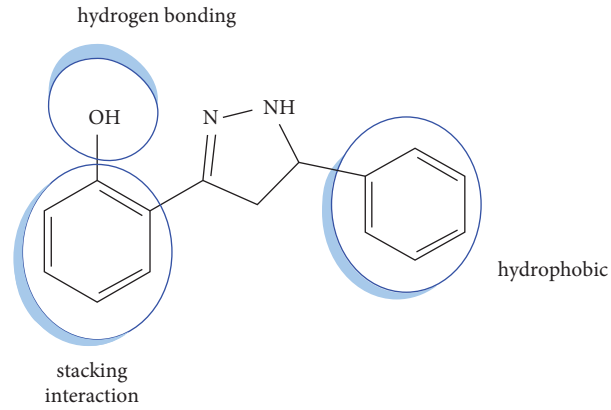

Figure 1: 3-(5-Hydroxyphenyl)-5-phenyl-2-pyrazolines have hydrogen bonding, stacking, and hydrophobic interaction groups.

Yield (339 mg, 59%). ^{1}H NMR (400 MHz, DMSO-d$_6$) δ 11.23 (s, 1H), 8.18 (d, J = 8.2 Hz, 1H), 7.97 (dd, J = 7.6, 1.7 Hz, 1H), 7.95 (d, J = 3.4 Hz, 1H), 7.86 (d, J = 8.1 Hz, 1H), 7.71 (d, J = 7.1 Hz, 1H), 7.64 (dd, J = 8.5, 1.0 Hz, 1H), 7.60 (dd, J = 8.3, 6.8, 1.6 Hz, 1H), 7.56 (dd, J = 8.3, 6.8, 1.6 Hz, 1H), 7.50 (td, J = 7.4 Hz, 1H), 7.27 (dd, J = 7.7, 1.5 Hz, 1H), 7.22 (dd, J = 8.4, 6.8, 1.6 Hz, 1H), 6.93 (dd, J = 8.2, 1.0 Hz, 1H), 6.85 (td, J = 7.5, 1.1 Hz, 1H), 5.61 (td, J = 10.7, 3.0 Hz, 1H), 3.92 (dd, J = 16.7, 11.2 Hz, 1H), and 2.96 (dd, J = 16.7, 10.4 Hz, 1H). ^{13}C NMR (100 MHz, DMSO-d$_6$) δ 156.72, 152.36, 137.98, 133.54, 130.50, 129.70, 128.68, 127.78, 127.62, 126.25, 125.76, 125.52, 123.58, 123.16, 119.13, 116.81, 115.71, 58.82, and 40.70. HRMS (ESI) m/z calcd for $C_{19}H_{16}N_2O$ $(M+H)^+$ 289.1341, found 289.1027.

$$5-(\text{naphthalene}-1-yl)-3-(2-\text{hydroxy}-6-\text{methoxyphenyl})\text{pyrazoline}. \quad (2)$$

Yield (356 mg, 56%). ^{1}H NMR (400 MHz, $CHCl_3$-d) δ 12.15 (s, 1H), 8.05 (d, J = 8.3 Hz, 1H), 7.89 (d, J = 7.4, 1.3 Hz, 1H), 7.79 (d, J = 8.2 Hz, 1H), 7.65 (d, J = 7.1 Hz, 1H), 7.57 (dd, J = 8.2, 6.8, 1.4 Hz, 1H), 7.52 (dd, J = 7.8, 7.0, 1.1 Hz, 1H), 7.45 (m, 1H), 7.14 (t, J = 8.3 Hz, 1H), 6.65 (dd, J = 8.3, 0.8 Hz, 1H), 6.36 (d, J = 8.1 Hz, 1H), 5.93 (br, s, 1H), 5.54 (t, J = 9.8 Hz, 1H), 3.96 (dd, J = 17.7, 10.7 Hz, 1H), 3.71 (s, 3H), and 3.41 (dd, 17.7, 9.0 Hz, 1H). ^{13}C NMR (100 MHz, $CHCl_3$-d) δ 159.65, 158.40, 153.92, 137.56, 133.96, 130.72, 130.36, 129.03, 128.09, 126.33, 125.74, 125.63, 122.96, 122.94, 109.93, 106.56, 101.48, 77.32, 77.00, 76.68, 59.02, 55.40, and 44.64. HRMS (ESI) m/z calcd for $C_{20}H_{18}N_2O_2$ $(M+H)^+$ 319.1447, found 319.1106.

$$5-(\text{naphthalene}-1-yl)-3-(2-\text{hydroxy}-4,6-\text{dimethoxyphenyl})\text{pyrazoline}. \quad (3)$$

Yield (299 mg, 43%). ^{1}H NMR (400 MHz, DMSO-d$_6$) δ 8.16 (d, J = 8.2 Hz, 1H), 7.95 (dd, J = 7.6, 1.4 Hz, 1H), 7.84 (d, J = 8.2 Hz, 1H), 7.70 (d, J = 7.1 Hz, 1H), 7.59 (m, 1H), 7.57 (m, 1H), 7.53 (m, 1H), 7.49 (*t*, J = 7.7 Hz, 1H), 6.15 (d, J = 2.3 Hz, 1H), 6.07 (d, J = 2.3 Hz, 1H), 5.49 (td, J = 10.6, 4.9 Hz, 1H), 3.95 (dd, J = 17.5, 10.9 Hz, 1H), 3.75 (s, 3H), 3.66 (s, 3H), and 3.04 (dd, J = 17.5, 10.9 Hz, 1H). ^{13}C NMR

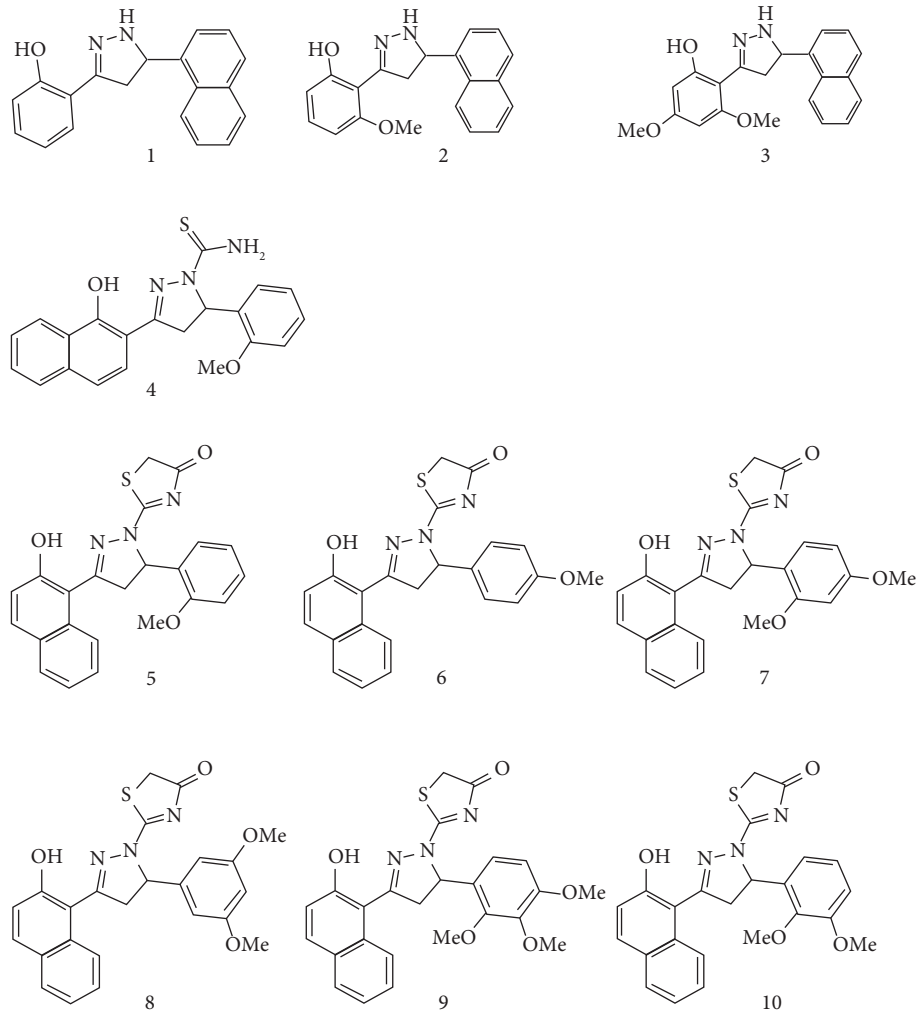

Figure 2: Structures of ten 3-(5-hydroxyphenyl)-5-phenyl-2-pyrazolines.

(100 MHz, DMSO-d_6) δ 161.16, 160.17, 158.93, 151.80, 138.46, 133.56, 130.57, 128.71, 127.51, 126.27, 125.74, 125.57, 123.53, 123.21, 100.06, 93.92, 90.51, 58.42, 55.65, 55.22, and 44.83. HRMS (ESI) m/z calcd. for $C_{21}H_{20}N_2O_3$ $(M+H)^+$ 349.1552, found 349.1169.

$$2-(5-(2,3-\text{dimethoxyphenyl})-3-(2-\text{hydroxynaphthalen}-1-yl)-4,5-\text{dihydropyrazol}-1-yl)\text{thiazol}-4(5H)-\text{one}. \quad (4)$$

Yield (339 mg, 76%). ^{1}H NMR (400 MHz, DMSO-d_6) δ 11.98 (s, 1H), 9.63 (d, J = 8.7 Hz, 1H), 7.95 (d, J = 8.9 Hz, 1H), 7.91 (d, J = 8.0 Hz, 1H), 7.59 (t, J = 7.8 Hz, 1H), 7.45 (t, J = 7.4 Hz, 1H), 7.21 (d, J = 9.2 Hz, 1H), 7.15 (d, J = 5.1 Hz, 1H), 7.14 (s, 1H), 7.10 (m, 1H), 5.56 (dd, J = 12.3, 3.0 Hz, 1H), 3.96 (s, 2H), 3.84 (s, 3H), 3.82 (dd, J = 16.5, 3.1 Hz, 1H), and 2.98 (dd, J = 16.4, 12.4 Hz, 1H). ^{13}C NMR (100 MHz, DMSO-d_6) δ 173.96, 163.58, 158.06, 157.53, 152.30, 145.82, 133.28, 132.86, 130.83, 129.57, 128.69, 128.01, 127.17, 124.29, 124.17, 119.05, 118.27, 113.00, 111.66, 72.34, 60.70, 55.81, 33.20, and 32.98. HRMS (ESI) m/z calcd. for $C_{24}H_{21}N_3O_4S$ $(M+H)^+$ 448.1331, found 448.1336.

High-resolution mass spectrometry was performed on an MS Q-TOF/G6550A (Agilent, Santa Clara, CA, USA) installed at the Korea Basic Science Institute (Seoul, Korea). Electrospray ionization and Q-TOF MS analysis were performed, and the gradient solvent system was a mixture of A (100% H_2O, 0.1% formic acid) and B (100% acetonitrile, 0.1% formic acid). The flow rate and injection volumes were 0.3 mL/min and 1 μL, respectively. Compounds were dissolved in dimethylsulfoxide-d6 for NMR experiments and transferred to 2.5 mm NMR tubes, and their concentrations were adjusted to approximately 50 mM. All NMR data were collected on a 700-spectrometer system (16.5 T; Bruker, Karlsruhe, Germany) at room temperature, and the chemical shifts were referenced to tetramethylsilane. The NMR and HR/MS spectra of compounds **1**, **2**, **3**, and **10** are provided in the Supplementary Materials (available here). The synthetic procedure for compounds **4**–**9** and their spectroscopic data, including NMR spectroscopy and high-resolution mass spectrometry, have been described elsewhere [22].

2.2. TLR7 Agonistic Activity Assay. To evaluate the effect of ten 3-(5-hydroxyphenyl)-5-phenyl-2-pyrazolines on TLR7 agonistic activity, we used HEK-Blue™ hTLR7 reporter cells (InvivoGen, San Diego, CA, USA), which stably overexpress human TLR7 and an NF-κB-inducible secreted embryonic alkaline phosphatase (SEAP) reporter gene to monitor TLR7 agonism. The reporter cells were treated with 50 μM derivatives. The TLR4 agonist lipopolysaccharide from *Porphyromonas gingivalis* (LPS-PG; InvivoGen) was used as a negative control, and known TLR7 agonists imiquimod (R837; InvivoGen) and resiquimod (R848; InvivoGen) were used as positive controls. After 24 h of incubation, TLR7-induced SEAP reporter activities were measured in the culture supernatant by reading the OD at 650 nm using a VersaMax microplate reader (Molecular Devices, CA, USA), according to the manufacturer's protocol (Invitrogen).

2.3. Cell Culture. THP-1 human monocytic leukemia cells were obtained from the American Type Culture Collection (Manassas, VA, USA) and cultured in Roswell Park Memorial Institute medium supplemented with 10% heat-inactivated fetal bovine serum (CellGro/Corning, Manassas, VA, USA) and 2 mM L-glutamine (Gibco BRL/Thermo Fisher Scientific, Waltham, MA, USA) in a humidified 5% CO_2 atmosphere at 37°C.

2.4. RT-PCR Analysis. Total RNA isolation and first-strand cDNA synthesis were performed as previously described [23]. The following RT-PCR primers were synthesized by Macrogen (Seoul, Republic of Korea): glyceraldehyde 3-phosphate dehydrogenase (GAPDH) forward, 5′-ACC CAC TCC ACC TTT G-3′; GAPDH reverse, 5′-CCC AGC AAG AGC ACA AGA G-3′; TNF-α forward, 5′-GAG TGA CAA GCC TGT AGC CCA TGT TGT-3′; TNF-α reverse, 5′-GCA ATG ATC CCA AAG TAG ACC TGC CCA GAC-3′; IL-1β forward, 5′-AAA CAG ATG AAG TGC TCC TTC CAG G-3′; IL-1β reverse, 5′-TGG AGA ACA CCA CTT GTT GCT CCA-3′. The PCR products were electrophoresed on a 1% agarose gel. The intensity of each band was quantified using Image J software (National Institutes of Health, Bethesda, MA, USA; https://imagej.nih.gov/ij/), normalized to GAPDH intensity, and expressed as a fold-increase relative to the unstimulated control.

2.5. In Silico Docking. In silico docking was performed using the AutoDock Vina program (The Scripps Research Institute, La Jolla, San Diego, USA) [24]. The three-dimensional (3D) structure of *Macaca mulatta* TLR7, deposited as 5 gmh·pdb in the protein data bank database, was used because it contains resiquimod as the ligand [25]. The binding site was determined using the grid box module provided by the AutoDock Tools program (ADT; Scripps Research Institute, La Jolla, San Diego, USA). The interactions between the protein and ligand inside the binding site were analyzed using the LigPlot program [26], and 3D images were generated using PyMOL software (PyMOL Molecular Graphics System, Version 1.0r1, Schrödinger, LLC). The holoprotein without ligands was obtained using the UCSF chimera visualization system [27]. The docking procedure was performed as previously reported [28]. The 3D structure of the ligand was obtained from energy minimization using Sybyl 7.3 (Tripos, St. Louis, MO) installed on an Intel Core 2 Quad Q6600 (2.4 GHz) Linux PC.

2.6. Statistical Analysis. Statistical significance was determined by one-way ANOVA followed by Sidak's multiple comparison test using GraphPad Prism version 9.3.1 (GraphPad Software Inc., La Jolla, CA, USA). Data are presented as the mean ± standard deviation (SD). Multiple group means were compared using Tukey's HSD test as a post hoc test. Statistical analyses were conducted using the IBM SPSS Statistics software (SPSS Inc., USA). A p value less than 0.05 was considered statistically significant.

3. Results and Discussion

The monomeric crystallographic structures of the TLR7 ligand complexes, including guanosine and polyuridine ssRNA (polyU), were demonstrated in the absence of the TLR7 ligand. However, they dimerize when ligands such as guanosine and polyU bind to TLR7 [25]. TLR7 contains two separate sites; the first accepts guanosine, and the second accepts polyU. The first site recognizes small molecules as ligands and can induce the dimerization of TLR7. In addition, dimerization occurs when a ligand binds to the first site, even if the ligand does not bind to the second site. TLR7 exists as a monomer in its resting state [20]. This phenomenon can be used to determine whether a compound binds to TLR7. Dimerization results in association with the adaptor protein myeloid differentiation primary response 88 (MyD88) and initiates signaling cascades that induce the transcription of inflammatory mediators [29]. The signaling pathways of TLR7 activate three transcriptional factors: NF-κB, AP-1, and IRF7. Monitoring the activation of NF-κB can help identify the stimulation of TLR7. Stimulation with a TLR7 ligand activates NF-κB and AP-1, which produce secreted embryonic alkaline phosphatases. Therefore, the detection of secreted embryonic alkaline phosphatases provides information about the dimerization of TLR7. The activation of TLR7 induced by 3-(5-hydroxyphenyl)-5-phenyl-2-pyrazolines compounds was measured using HEK-Blue™ hTLR7 reporter cells. For comparison, the TLR4 agonist LPS-PG was used as a negative control, and imiquimod and resiquimod were used as positive controls. First, testing whether TLR7 was activated using compounds **1**, **2**, **3**, **4**, **5**, and **9** confirmed that compounds **5** and **9** significantly activated TLR7 (Figure 3(a)). Imiquimod and resiquimod had significantly higher TLR7 activation levels than all other compounds. Compounds **5** and **9** had the same backbone but different moieties; therefore, additional confirmatory experiments were performed using six analogue compounds **5**–**10**. A half maximal effective concentration (EC_{50}) value of each compound was 15–80 μM

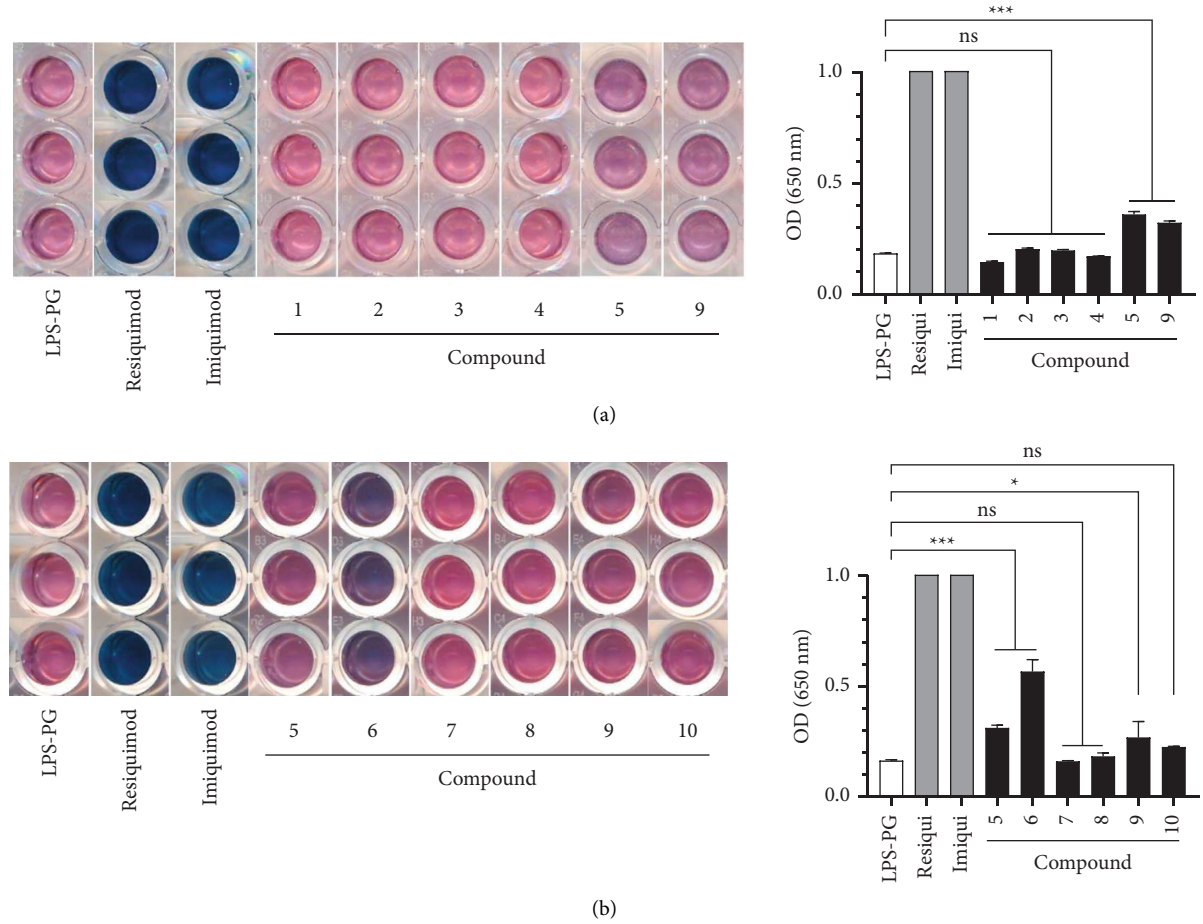

Figure 3: Effect of 3-(5-hydroxyphenyl)-5-phenyl-2-pyrazolines derivatives on TLR7 agonist activity: (a) HEK-Blue hTLR7 reporter cells were treated with compounds **1**, **2**, **3**, **4**, **5**, and **9** (top panel) or compounds **5**, **6**, **7**, **8**, **9**, and **10** (bottom panel) at 50 μM for 24 h and (b) TLR7-induced secreted embryonic alkaline phosphatase (SEAP) reporter activities were measured with the culture supernatant by reading the OD at 650 nm using a VersaMax microplate reader. LPS-PG was used as a negative control, whereas 2.9 μM resiquimod and imiquimod were used as positive controls. ns: not significant, $^{*}p < 0.05$ and $^{***}p < 0.001$.

(Supplementary Figure 5). Among the compounds tested, compound **6** showed the best activity when treated at a concentration of 50 μM (Figure 3(b)).

To assess the agonistic activity of compound **6** on TLR7, we examined its effect on the TLR7-mediated signaling pathway. THP1 human monocytic cells were treated with 40 μM compound **6** for different periods, and the phosphorylation status of TLR7 downstream effectors was determined using immunoblot analysis. We found that treatment with compound **6** rapidly induced the phosphorylation of IRAK4 at Thr345/Ser346, IKKα/β at Ser176/180, IκBα at Ser32, and p65/RelA at Ser536 within 10 min of exposure (Figures 4(a) and 4(b)). Phosphorylated NF-κB in the nucleus is recognized as a marker of NF-κB-mediated transcriptional activation. To further address the effect of compound **6** on TLR7 agonistic activity, we examined the localization of phosphorylated p65/RelA NF-κB using immunofluorescence microscopy. Phosphorylated p65/RelA at Ser536 was detected in the nucleus after treatment with compound **6** via immunostaining (Figure 4(c)). These data suggest that compound **6** exhibits TLR7 agonistic activity.

TLR7 stimulates the expression of various innate cytokines, including TNF-α and IL-1β, via NF-κB [30]. We next examined whether compound **6** affected the expression of NF-κB-targeted innate cytokines in THP1 cells. EC_{50} values of resiquimod and compound **6** for stimulating IL1β and TNFα mRNA expression were calculated using a quantitative real-time PCR analysis. Resiquimod showed EC_{50} values of 0.2612 μM and 1.337 μM for IL1β and TNFα mRNA expression, respectively (Supplementary Figure 6(a)), whereas EC_{50} values of compound **6** were 8.482 μM and 1.95 μM for IL1β and TNFα mRNA expression, respectively (Supplementary Figure 6(b)). RT-PCR analysis showed that upon exposure to 40 μM compound **6**, TNFα and IL1β mRNA levels substantially increased within 3 h and remained elevated for at least 12 h and 24 h, respectively (Figure 5(a)). Densitometric analysis revealed that TNFα mRNA levels were increased by 2.77 ± 0.301, 2.46 ± 0.221, 1.74 ± 0.0551, and 0.810 ± 0.385 fold after 3, 6, 12, and 24 h of compound **6** stimulation, respectively, as compared to that of the control. Additionally, IL1β mRNA levels were increased by 3.42 ± 0.288, 3.63 ± 0.208, 3.43 ± 0.418, and 2.55 ± 0.409 fold after 3, 6, 12, and 24 h of compound **6**

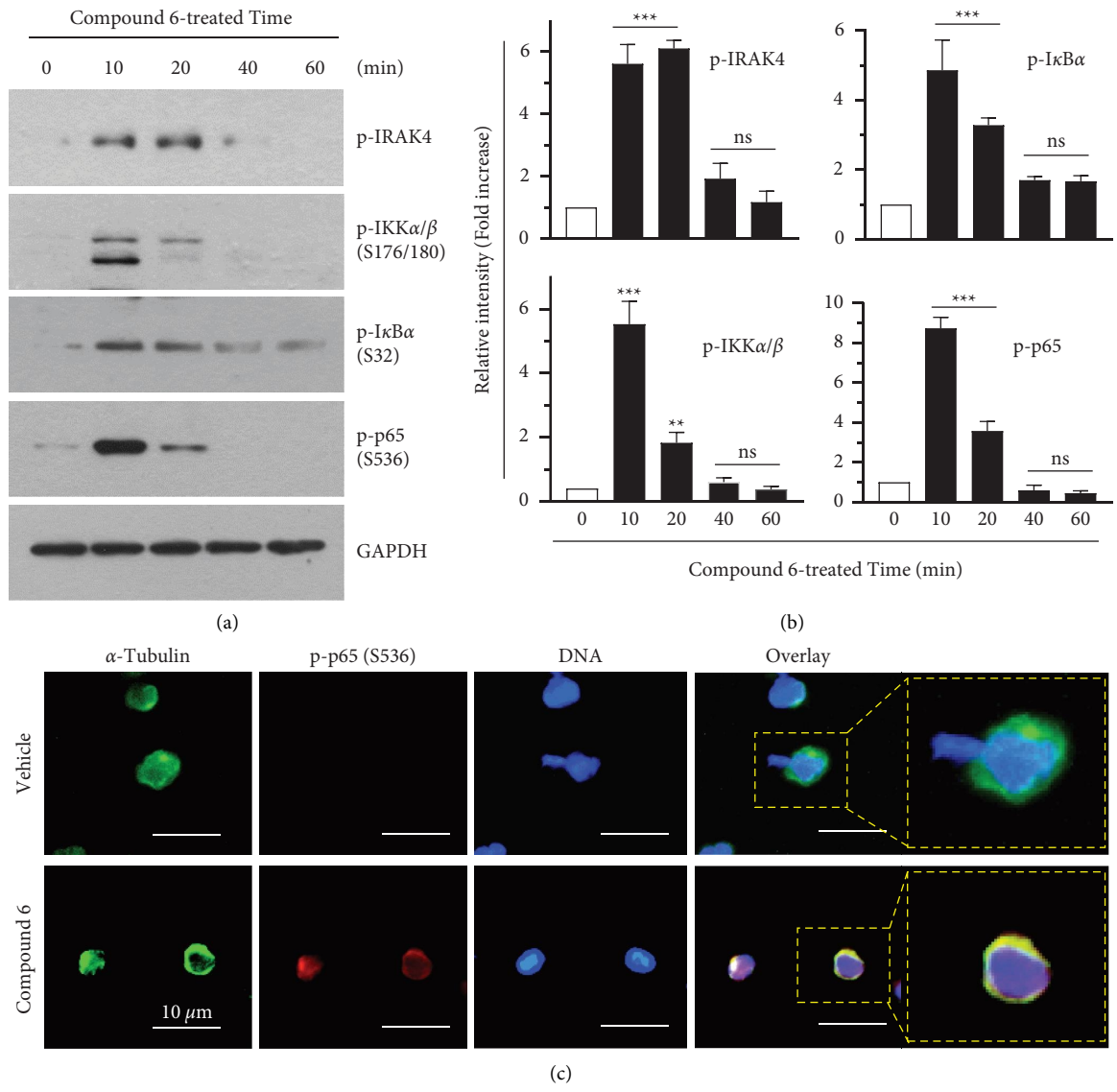

Figure 4: TLR7 agonist activity of compound **6**. (a) Images of SEAP assay plates. THP1 cells were treated with 40 μM compound **6** for different durations. Whole-cell lysates were immunoblotted with antibodies against phospho-IRAK4 (Thr345/Ser346), −IKKα/B (Ser176/180), −IκBα (Ser32), and -p65/RelA NF-κB (Ser536). GAPDH level was used as an internal control. (b) Protein band intensities were measured using Image J software. The data are presented as means ± SD ($n = 3$). ns: not significant, $^{**}p < 0.01$, and $^{***}p < 0.001$. (c) THP1 cells were treated with 40 μM compound **6** for 10 min and then incubated with an antibody against p-p65/RelA (Ser536) or α-tubulin for 2 h followed by the addition of Alexa Fluor 555-(red fluorescence for p-p65) or Alexa Fluor 488-(green fluorescence for α-tubulin) secondary antibody for an additional 30 min. Nuclear DNA was stained with 0.1 μg/mL Hoechst 33258 (blue fluorescence) for 10 min. Fluorescent cells were captured using an EVOSf1® fluorescence microscope. Bars, 10 μm.

stimulation, respectively, as compared to that of the control (Figure 5(b)). These data suggest that compound **6** promotes the production of innate cytokines regulated by NF-κB in THP1 monocytic cells.

To elucidate the mode of binding between compound **6** and TLR7, *in silico* docking analysis was performed. Because the 3D structure of TLR7 from *Homo sapiens* has not yet been reported, we used the monkey (*Macaca mulatta*) TLR7 structure containing resiquimod as a ligand (5 gmh·pdb) for *in silico* docking analysis. *Macaca mulatta* TLR7 consists of 1048 residues. The X-ray crystallographic structure of 5 gmh·pdb comprises homodimeric polypeptides A and B, containing 799 residues (Arg36–Leu834) and two resiquimod ligands. The LigPlot analysis (Supplementary Figure 7) shows that residues surrounding resiquimod belong to both A and B chains; a 3D structure containing homodimeric polypeptides A and B was used, and its holoprotein was prepared by deleting resiquimod using the UCSF chimera visualization system. The binding sites for the docking experiments were determined using the grid box module of the AutoDock Tools program as follows: the centers of x, y, and z were −12.972, −26.750, and −12.083, respectively, and their sizes were 22, 22, and 24, respectively. To confirm the accuracy of the current docking procedure, resiquimod, the ligand included in

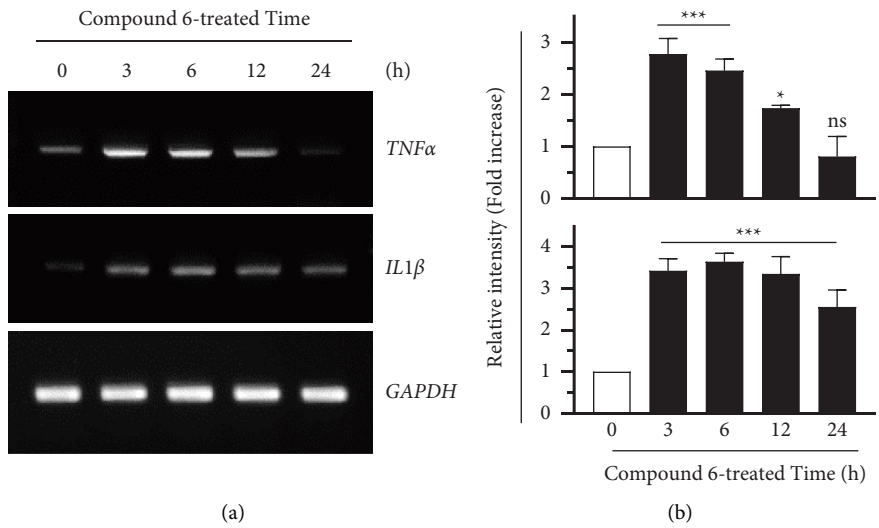

Figure 5: Effect of compound **6** on TLR7-mediated innate cytokines expression. THP1 cells were treated with 40 μM compound **6** for various periods (0–24 h). (a) TNFα and IL1β mRNA levels were determined using RT-PCR (a). GAPDH mRNA levels were used as an internal control. (b) PCR band intensities were measured using the Image J software. Bars represent the mean ± S.D. ($n = 3$). ns: not significant, $^{*}p < 0.05$, and $^{***}p < 0.001$ by Dunnett's multiple comparisons test.

5 gmh·pdb, was docked into the holoprotein prepared as described previously. The ligand obtained from the current docking process was superimposed on the ligand contained in 5 gmh·pdb. Supplementary Figure 8 shows that they match well with each other. Its binding energy ranged from −6.0 to −9.0 kcal/mol. The 3D structure of compound **6** was determined based on the 3D structure of (2R,5R)-1-(3,4-dihydro-2H-pyrrol-5-yl)-2,5-diphenylpyrrolidine deposited in PubChem (CID 146163719). Similar to resiquimod, compound **6** was docked into the holoprotein. Its binding energy ranged from −5.1 to −7.9 kcal/mol. As the docking procedure was iterated nine times, nine docking results were generated. The holoprotein-compound**6** complex with the best docking pose and lowest binding energy was selected. Compound **6**, residing in the binding site, was compared with resiquimod in 5 gmh·pdb (Figure 6).

As shown in this image, with resiquimod in the binding site, compound **6** spanned the entrance and the inside of the binding site. The LigPlot analysis demonstrated that oxygen of the carbonyl group of Gln354(B) is close to the nitrogen of thiazolone of compound **6** to form a hydrogen bond (2.93 Å). Eight residues, including Tyr264(B), Phe351(B), Val355(B), Tyr356(B), Phe408(B), Leu557(A), His558(A), and Thr586(A) participate in hydrophobic interactions with compound **6** (Figure 7). Here, A and B in parentheses denote TLR7 homodimeric polypeptides A and B, respectively. In resiquimod, 11 residues, including Tyr264(B), Phe349(B), Phe351(B), Val355(B), Tyr356(B), Val381(B), Phe408(B), Thr532(A), Leu557(A), Ile585(A), and Thr586(A), participate in hydrophobic interactions with resiquimod (Supplementary Figure 7).

Two oxygens of the carboxyl group of Asp555(A) are proximal to nitrogens of resiquimod (2.53 and 2.71 Å). Three more residues interacted with resiquimod than with compound **6**. The benzene ring of resiquimod was stacked on the benzene ring of F408, but no stacking interactions were

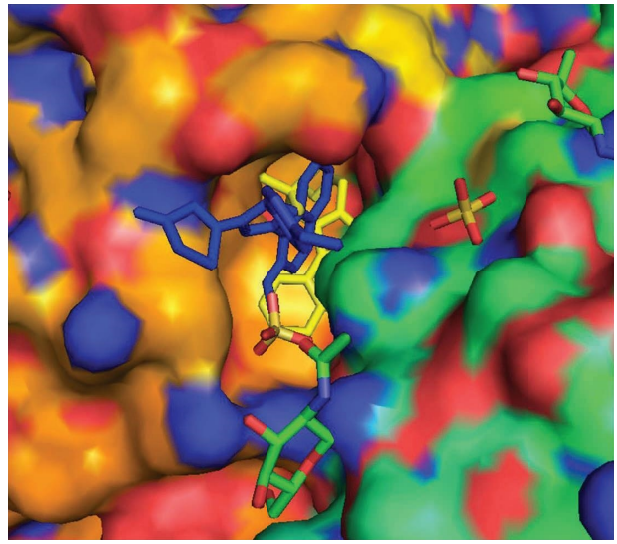

Figure 6: Compound **6** (blue color) residing in the binding site superimposed with resiquimod (yellow color) contained in 5 gmh·pdb.

observed between compound **6** and any residue (Figure 8). As mentioned in the introduction, among pharmacophores, including hydrogen bonding, stacking, hydrophobic, and van der Waals interactions, stacking interactions were missing in compound **6** [20]. In addition, with resiquimod in the binding pocket, compound **6** spanned the entrance of the binding site to the inside (Figure 6). This phenomenon may result in lower binding energy between resiquimod and TLR7 than that of compound **6**. The title compound, 2-(3-(2-hydroxynaphthalen-1-yl)-5-(4-methoxyphenyl)-4,5-dihydro-1H-pyrazol-1-yl)thiazol-4(5H)-one, consists of 2-pyrazoline and thiazolone moieties instead of the 1H-imidazo(4,5-c)pyridine contained in resiquimod.

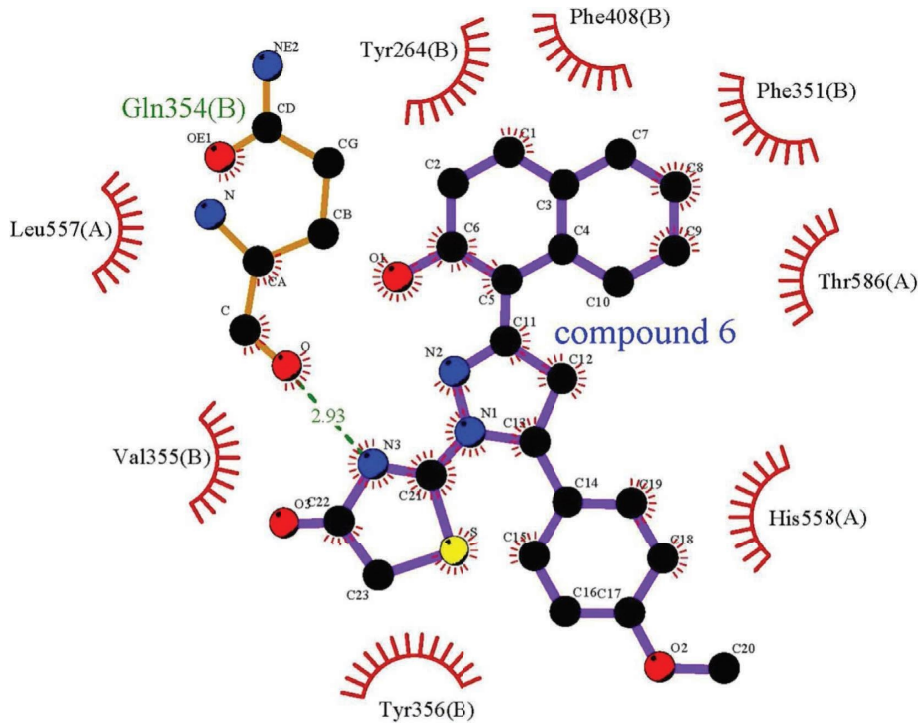

Figure 7: LigPlot analysis of the compound **6**-TLR7 complex. The oxygen of the carbonyl group of Gln354(B) is close to the thiazolone nitrogen of compound 6 (2.93 Å). Eight residues, including Tyr264 (B), Phe351(B), Val355(B), Tyr356(B), Phe408(B), Leu557(A), His558(A), and Thr586(A), participate in hydrophobic interactions with compound **6**.

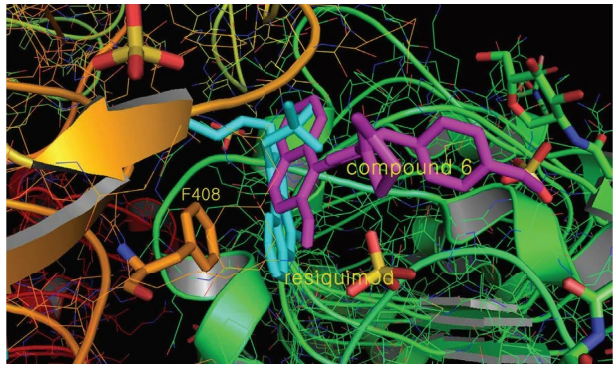

Figure 8: Benzene ring of resiquimod (cyan color) is stacked with the benzene ring of F408. Nevertheless, compound **6** (magenta color) is not stacked because its naphthalene faces diagonally instead of facing side by side with F408.

4. Conclusions

Based on TLR7-induced secreted embryonic alkaline phosphatase reporter activity assay, TLR7 was activated by compounds with 2-pyrazoline and thiazolone moieties. The title compound promoted the production of innate cytokines regulated by NF-κB in THP1 monocytic cells. In conclusion, diverse TLR7 agonists can be developed based on the current results.

Data Availability

The data are available from the corresponding author upon reasonable request.

Conflicts of Interest

The authors declare that they have no conflicts of interest.

Acknowledgments

This work was supported by the KU Research Professor Program of Konkuk University. This work was supported by the Basic Science Research Program through the National Research Foundation of Korea (NRF), funded by the Ministry of Science, ICT and Future Planning (grant no. NRF-2020R1A2C1005845).

Supplementary Materials

The NMR and HR/MS spectra of compounds **1**, **2**, **3**, and **10**. Supplementary Figure 1: structures of (a) imiquimod (R-837), (b) resiquimod (R-848), and (c) PF-4878691. Supplementary Figure 2: (a) 2-imidazoline and (b) 2-pyrazoline. Supplementary Figure 3: (a) in resiquimod, oxygen is located at a distance of 2.8 Å and 3.5 Å from nitrogen and (b) for 3-(5-hydroxyphenyl)-5-phenyl-2-pyrazoline, oxygen occurs at a distance of 2.6 Å and 3.8 Å from nitrogen. Supplementary Figure 4: the synthetic scheme for compounds **1**, **2**, **3**, and **10**. Supplementary Figure 5: half maximal effective concentration (EC_{50}) values of compounds **5**–**10**. Supplementary Figure 6: (a) Resiquimod showed EC_{50} values of 0.2612 μM and 1.337 μM for IL1β and TNFα mRNA expression, respectively, and (b) EC_{50} values of compound **6** were 8.482 μM and 1.95 μM for IL1β and TNFα mRNA expression, respectively. Supplementary Figure 7: resiquimod contained in the X-ray crystallographic structure of TLR7 (5 gmh·pdb) as a ligand and residues residing in its binding site analyzed by the LigPlot program. Supplementary Figure 8: the 3D image of resiquimod docked into the holoprotein of TLR7 generated using the PyMOL program. (*Supplementary Materials*)

References

[1] S. Akira, "Toll-like receptors and innate immunity," *Advances in Immunology*, vol. 78, pp. 1–56, 2001.

[2] A. Aderem and R. J. Ulevitch, "Toll-like receptors in the induction of the innate immune response," *Nature*, vol. 406, no. 6797, pp. 782–787, 2000.

[3] S. Akira, K. Takeda, and T. Kaisho, "Toll-like receptors: critical proteins linking innate and acquired immunity," *Nature Immunology*, vol. 2, no. 8, pp. 675–680, 2001.

[4] A. Iwasaki and R. Medzhitov, "Toll-like receptor control of the adaptive immune responses," *Nature Immunology*, vol. 5, no. 10, pp. 987–995, 2004.

[5] S. Adams, "Toll-like receptor agonists in cancer therapy," *Immunotherapy*, vol. 1, no. 6, pp. 949–964, 2009.

[6] K. Crozat and B. Beutler, "TLR7: a new sensor of viral infection," *Proceedings of the National Academy of Sciences*, vol. 101, no. 18, pp. 6835-6836, 2004.

[7] J. Lee, C. C. N. Wu, K. J. Lee et al., "Activation of anti-hepatitis C virus responses via Toll-like receptor 7," *Proceedings of the National Academy of Sciences*, vol. 103, no. 6, pp. 1828–1833, 2006.

[8] J. Lee, T.-H. Chuang, V. Redecke et al., "Molecular basis for the immunostimulatory activity of guanine nucleoside analogs: activation of Toll-like receptor 7," *Proceedings of the National Academy of Sciences*, vol. 100, no. 11, pp. 6646–6651, 2003.

[9] K. Poulas, K. Farsalinos, and C. Zanidis, "Activation of TLR7 and innate immunity as an efficient method against COVID-19 pandemic: imiquimod as a potential therapy," *Frontiers in Immunology*, vol. 11, p. 1373, 2020.

[10] M. D. Fidock, B. E. Souberbielle, C. Laxton et al., "The innate immune response, clinical outcomes, and ex vivo HCV antiviral efficacy of a TLR7 agonist (PF-4878691)," *Clinical Pharmacology & Therapeutics*, vol. 89, no. 6, pp. 821–829, 2011.

[11] L. Englmeier and J. Subburayalu, "What's happening where when SARS-CoV-2 infects: are TLR7 and MAFB sufficient to explain patient vulnerability?" *Immunity & Ageing*, vol. 19, no. 1, p. 6, 2022.

[12] C. I. Van Der Made, A. Simons, J. Schuurs-Hoeijmakers et al., "Presence of genetic variants among young men with severe COVID-19," *Journal of the American Medical Association*, vol. 324, no. 7, pp. 663–673, 2020.

[13] P. H. Goff, T. Hayashi, L. Martínez-Gil et al., "Synthetic Toll-like receptor 4 (TLR4) and TLR7 ligands as influenza virus vaccine adjuvants induce rapid, sustained, and broadly protective responses," *Journal of Virology*, vol. 89, no. 6, pp. 3221–3235, 2015.

[14] A. J. Smith, Y. Li, H. G. Bazin et al., "Evaluation of novel synthetic TLR7/8 agonists as vaccine adjuvants," *Vaccine*, vol. 34, no. 36, pp. 4304–4312, 2016.

[15] H. Hemmi, T. Kaisho, O. Takeuchi et al., "Small anti-viral compounds activate immune cells via the TLR7 MyD88–dependent signaling pathway," *Nature Immunology*, vol. 3, no. 2, pp. 196–200, 2002.

[16] T. W. Kim, K. Staschke, K. Bulek et al., "A critical role for IRAK4 kinase activity in Toll-like receptor–mediated innate immunity," *Journal of Experimental Medicine*, vol. 204, no. 5, pp. 1025–1036, 2007.

[17] J. Inoue, J. Gohda, and T. Akiyama, "Characteristics and Biological Functions of TRAF6," *TNF Receptor Associated Factors (TRAFs)*, pp. 72–79, Springer, Berlin, Germany, 2007.

[18] J. Šedý, V. Bekiaris, and C. F. Ware, "Tumor necrosis factor superfamily in innate immunity and inflammation," *Cold Spring Harbor Perspectives in Biology*, vol. 7, no. 4, Article ID 16279, 2014.

[19] H. Yu, Z. Wang, G. Sun, and Y. Yu, "Recognition of nucleic acid ligands by toll-like receptors 7/8: importance of chemical modification," *Current Medicinal Chemistry*, vol. 19, no. 9, pp. 1365–1377, 2012.

[20] S. Bhagchandani, J. A. Johnson, and D. J. Irvine, "Evolution of Toll-like receptor 7/8 agonist therapeutics and their delivery approaches: from antiviral formulations to vaccine adjuvants," *Advanced Drug Delivery Reviews*, vol. 175, Article ID 113803, 2021.

[21] W. Chanput, J. J. Mes, and H. J. Wichers, "THP-1 cell line: an in vitro cell model for immune modulation approach," *International Immunopharmacology*, vol. 23, no. 1, pp. 37–45, 2014.

[22] D. Koh, S. Y. Shin, J. Sung, S. Ahn, and Y. Lim, "1H and 13C NMR spectral assignments for 24 novel naphthalenylphenylpyrazolines," *Magnetic Resonance in Chemistry*, vol. 55, no. 9, pp. 856–863, 2017.

[23] S. Y. Shin, C. G. Kim, Y. J. Jung, Y. Lim, and Y. H. Lee, "The UPR inducer DPP23 inhibits the metastatic potential of MDA-MB-231 human breast cancer cells by targeting the Akt–IKK–NF-κB–MMP-9 axis," *Scientific Reports*, vol. 6, no. 1, Article ID 34134, 2016.

[24] O. Trott and A. J. Olson, "AutoDock Vina: improving the speed and accuracy of docking with a new scoring function,

efficient optimization, and multithreading," *Journal of Computational Chemistry*, vol. 31, no. 2, pp. 455–461, 2010.

[25] Z. Zhang, U. Ohto, T. Shibata et al., "Structural analysis reveals that Toll-like receptor 7 is a dual receptor for guanosine and single-stranded RNA," *Immunity*, vol. 45, no. 4, pp. 737–748, 2016.

[26] B. Kramer, M. Rarey, and T. Lengauer, "Evaluation of the FLEXX incremental construction algorithm for protein–ligand docking," *Proteins: Structure, Function, and Genetics*, vol. 37, no. 2, pp. 228–241, 1999.

[27] E. F. Pettersen, T. D. Goddard, C. C. Huang et al., "UCSF Chimera—a visualization system for exploratory research and analysis," *Journal of Computational Chemistry*, vol. 25, no. 13, pp. 1605–1612, 2004.

[28] Y. W. Song, Y. Lim, and S. K. Cho, "2, 4-Di-tert-butylphenol, a potential HDAC6 inhibitor, induces senescence and mitotic catastrophe in human gastric adenocarcinoma AGS cells," *Biochimica et Biophysica Acta, Molecular Cell Research*, vol. 1865, no. 5, pp. 675–683, 2018.

[29] S. Janssens and R. Beyaert, "A universal role for MyD88 in TLR/IL-1R-mediated signaling," *Trends in Biochemical Sciences*, vol. 27, no. 9, pp. 474–482, 2002.

[30] H. Matsushima, N. Yamada, H. Matsue, and S. Shimada, "TLR3-TLR7-and TLR9-mediated production of proinflammatory cytokines and chemokines from murine connective tissue type skin-derived mast cells but not from bone marrow-derived mast cells," *The Journal of Immunology*, vol. 173, no. 1, pp. 531–541, 2004.